Precision Measurements of the n-p Total Cross Section at 0.4926 and 3.205 MeV*

C. E. ENGELKE, R. E. BENENSON, E. MELKONIAN, AND J. M. LEBOWITZ
Columbia University, New York, New York
(Received 5 July 1962)

The n-p total cross section at 0.4926 MeV has been measured to be 6.202 b $\pm 0.18\%$. This measurement when combined with the latest results at zero energy, determines the n-p singlet effective range to be $(2.46\pm 0.12)\times 10^{-13}$ cm. The uncertainty has been decreased by a factor of 2 from the best previous determination. The systematic uncertainty due to shape dependence effects is less than $\pm 0.04\times 10^{-13}$ cm. The total n-p cross section at 3.205 MeV has been measured as 2.206 b $\pm 0.31\%$. This preliminary value was obtained in the process of measuring rate dependence effects to correct the n-p cross section at 0.4926 MeV for count rate dependence. The use of resonant (n,p) and (n,α) reactions for neutron detection in high-pressure gas scintillators is the most novel feature of the experimental method. An analysis is made of the propagation of the uncertainties in the various independent low-energy experiments into uncertainties in the calculated shape-independent cross section. The results of the analysis are presented as plots of percent cross section uncertainty versus neutron lab energy.

I. INTRODUCTION

THE nature of the two-nucleon interaction is a fundamental problem in nuclear physics, and the scattering of neutrons by hydrogen is one of the primary sources of information about this interaction. The most accurate quantative data are obtained at energies below about 25 MeV in which range monoenergetic neutrons of accurately known energy are available. In this energy region the data can be interpreted rather simply because S-wave scattering is predominant. To this extent the total (n,p) cross section can be written as $(3\pi/k^2)\sin^2\delta_t+(\pi/k^2)\sin^2\delta_S$, where δ_t is triplet S-wave phase shift, δ_s is singlet S-wave phase shift, and k is neutron wave number. At energies above 10 MeV, however, some correction for P- and D-wave scattering must be made to obtain the S-wave phase shifts from the measured total cross sections.

Landau[1] and Schwinger[2] have shown that the expansion of the quantity $k\cot\delta$ as a power series in k^2 furnishes a useful parametric representation of the S-wave $(n$-$p)$ total scattering cross section. The same type of expansion can be made for both the triplet and singlet phase shifts. If just three terms are retained in each of the two expansions, the total n-p cross section for S wave scattering can be written in terms of six parameters:

$$\sigma=\frac{3\pi}{k^2+[1/a_t-(k^2/2)r_{0t}(1-2P_tr_{0t}^2k^2)]^2}+\frac{\pi}{k^2+[1/a_s-(k^2/2)r_{0s}(1-2P_sr_{0s}^2k^2)]^2}. \quad (1)$$

The six parameters are: the scattering lengths, a_t and a_s; the effective ranges r_{0t} and r_{0s}; and the shape parameters P_t and P_s, where the subscripts t and s stand for triplet and singlet, respectively. It is through these six parameters that theory and experiment are most conveniently compared. Recently, the effective range expansion has been related to partial wave nucleon-nucleon dispersion relations.[3] This approach allows the parameters to be directly compared to meson theory without recourse to the nonrelativistic Schrödinger equation. The dispersion relation approach indicates that the three-term expansion is good only up to 10 MeV lab energy. Up to 40 MeV an accurate expression is obtained if a "shape function" $P(K^2)=P/(1+DK^2)$ is substituted for P in Eq. (1).

The results of many experiments must be combined to determine the parameters. A measurement of the free proton cross section with epithermal neutrons gives the sum of the weighted squares of the triplet and singlet scattering lengths at zero energy.[4] The "liquid mirror" experiment[5,6] determines the coherent scattering amplitude, which gives the algebraic sum of the weighted singlet and triplet scattering lengths. Combining these two experimental results then gives separate values for the triplet and singlet scattering lengths. The measurement of the binding energy ϵ_d of the deuteron combined with the value of triplet scattering length gives the triplet effective range at the binding energy of the deuteron.[7] In summary these results and their standard deviations are shown in Table I.

The problem of extracting the remaining three parameters r_{0s}, P_s, and P_t from additional precise total cross-section measurements may be divided into two parts, first the determination of r_{0s}, and then the determination of P_s and P_t. At a sufficiently low neutron energy the total cross section will be essentially independent of P_s and P_t, so that r_{0s} may be determined by a single cross-section measurement. This value may then be inserted into Eq. (1) and measurements of the

* Work partially supported by U. S. Atomic Energy Commission.
[1] L. D. Landau and Smorodensky, J. Phys. (U.S.S.R.) 8, 154 (1944).
[2] J. Schwinger, Harvard Lecture Notes (unpublished).
[3] H. P. Noyes and D. Y. Wong, Phys. Rev. Letters 3, 191 (1959); M. Cini, S. Fubini, and A. Stanghellini, Phys. Rev. 114, 1633 (1959).
[4] E. Melkonian, Phys. Rev. 76, 1744 (1949).
[5] M. T. Burgy, G. R. Ringo, and D. J. Hughes, Phys. Rev. 84, 1160 (1951).
[6] W. C. Dickinson, L. Passell, and O. Halpern, University of California Radiation Laboratory Report UCRL-6616 (unpublished).
[7] E. L. Chupp, R. W. Jewell, and W. John, Phys. Rev. 121, 234 (1961).

TABLE I. Values used for the zero-energy properties of the (n,p) system and the effective range parameters resulting from these values.

$\sigma_0=20.36\pm0.05$ b[a]
$a_c=-3.739\pm0.012$ F
$\epsilon_d=2.226\pm0.002$ MeV
$a_t=5.400\pm0.011$ F
$a_s=-23.677\pm0.029$ F
$r_{0t}(-\epsilon_d)=1.732\pm0.014$ F

[a] This uncertainty is less than that quoted in reference 4, where the uncertainty quoted in a conservative (2) × (standard deviation).

total (n,p) cross section at appropriate higher energies can furnish values of P_T and P_s.

In order to decide how to obtain the best accuracy in r_{0s}, one must first consider how the uncertainties in σ_0, $a_{\rm coh}$, ϵ_d, and the measured cross section σ propagate into uncertainties in r_{0s}. Figure 1 shows the over-all uncertainty in the value of r_0 singlet versus the energy E at which the cross-section measurement is made. Curves are drawn for the cases where the uncertainty in the cross-section measurement is 0.0, 0.1, 0.2, 0.3, and 0.4%. These curves are computed from the derivatives of the function $\sigma(E)$ with respect to the independent experimental parameters, e.g.,

$$(dr_{0s})^2=\frac{1}{(\partial\sigma/\partial r_{0s})^2}\left[(d\sigma)^2+\left(\frac{\partial\sigma}{\partial\sigma_0}d\sigma_0\right)^2+\left(\frac{\partial\sigma}{\partial a_{\rm coh}}da_{\rm coh}\right)^2+\left(\frac{\partial\sigma}{\partial\epsilon_d}d\epsilon_d\right)^2\right], \quad (2)$$

where

$$\frac{\partial\sigma}{\partial\sigma_0}=\frac{\partial\sigma}{\partial a_t}\frac{\partial a_t}{\partial\sigma_0}+\frac{\partial\sigma\partial a_s}{\partial a_s\partial\sigma_0}+\frac{\partial\sigma}{\partial r_{0t}}\frac{\partial r_{0t}}{\partial\sigma_0},$$

etc.

The conclusion drawn from Fig. 1 is that an energy near 0.4 MeV is particularly suitable to obtain r_{0s} most precisely. Shape dependence should be very small at this low energy, while the precision obtained in the singlet effective range for a given cross section accuracy

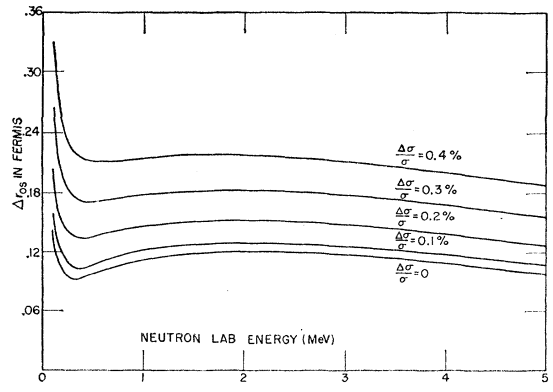

FIG. 1. Over-all uncertainty obtainable on r_{0s} as a function of the precision and energy of the determining cross-section measurement.

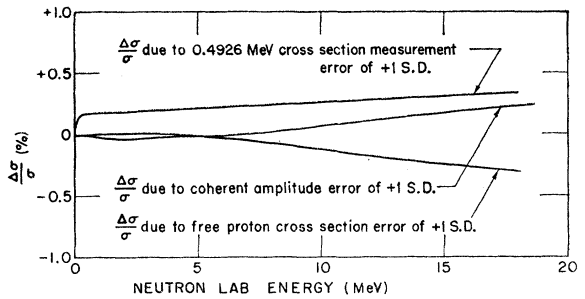

FIG. 2. Energy dependence of the uncertainties in the calculated shape-independent cross section due to the free proton cross-section uncertainty, the coherent amplitude uncertainty and the uncertainty in the present cross-section measurement at 0.4926 MeV. The effect of the uncertainty in ϵ_d is negligible.

is nearly optimum. The best previous determinations of r_{0s} where based on cross-section measurements of about $\pm0.4\%$ uncertainty at energies of 1.0 and 1.3 MeV. The value of r_{0s} obtained had random uncertainties of ±0.22 F and possible systematic errors of ±0.10 F due to unknown shape dependence effects. A cross-section measurement at about 0.4 MeV would determine r_{0s} with an ambiguity of less than ±0.04 F due to shape dependence effects. After an analysis of the experimental factors involved, a precision of $\pm0.2\%$ was judged feasible, which would give r_{0s} to ±0.12 F.

The second part of the problem is to attempt to extract P_t and P_s from total cross-section measurements at selected energies. First of all, the effect of the uncertainties in the values of the zero-energy cross section, coherent amplitude, binding energy of the deuteron, and in the cross-section measurement which determines r_{0s}, must be considered. Figure 2 shows to what extent an error of one standard deviation in each of these measurements causes deviations in the cross section calculated from the shape-independent approximation, $P_t=P_s=0$. The calculation is similar to that for Fig. 1. For example, the change in the predicted cross section due to an error $d\sigma_0$ is

$$(d\sigma)=\left[\frac{\partial\sigma}{\partial a_t}\frac{\partial a_t}{\partial\sigma_0}+\frac{\partial\sigma}{\partial a_s}\frac{\partial a_s}{\partial\sigma_0}+\frac{\partial\sigma}{\partial r_{0t}}\frac{\partial r_{0t}}{\partial\sigma_0}+\frac{\partial\sigma}{\partial r_{0s}}\frac{\partial r_{0s}}{\partial\sigma_0}\right]d\sigma_0. \quad (3)$$

Between 1953 and 1958 six precision measurements of the n-p total cross section were reported at energies ranging from 1.0 to 19.6 MeV.[8–12] The uncertainties in all these measurements were about $\pm0.4\%$, and these uncertainties were the major sources of uncertainty in the n-p singlet effective range. Furthermore, the experimental uncertainties were slightly too large to

[8] E. M. Hafner, W. F. Hornyak, C. E. Falk, G. Snow, and T. Coor, Phys. Rev. **89**, 204 (1953).
[9] R. E. Fields, R. L. Becker, and R. K. Adair, Phys. Rev. **94**, 389 (1954).
[10] C. L. Storrs and D. H. Frisch, Phys. Rev. **95**, 1252 (1954).
[11] H. L. Poss, E. V. Salant, G. A. Snow, and Luke C. L. Yuan, Phys. Rev. **87**, 11 (1952).
[12] R. B. Day, R. L. Mills, J. E. Perry, Jr., and F. Sherb, Phys. Rev. **114**, 209 (1959).

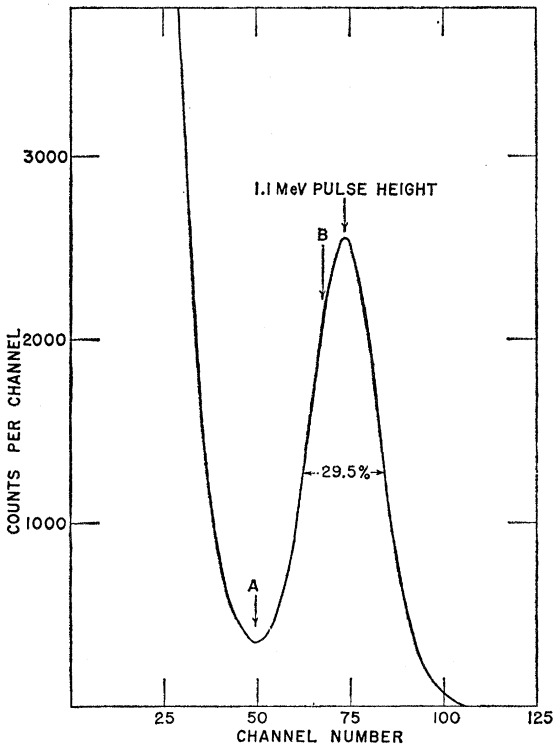

FIG. 3. Pulse-height spectrum caused by 0.5-MeV neutrons on a gas scintillation counter filled to 100 psi N_2 plus 400 psi xenon. The peak is due to protons from the $N^{14}(n,p)C^{14}$ reaction which are stopped in the active volume.

allow the extraction of meaningful information about the shape dependent parameters. Therefore, a program was initiated at Columbia University to perform a series of measurements of the neutron proton total cross section to accuracies better than $\pm 0.2\%$. This article reports:

(1) the development of experimental techniques capable of achieving the desired precision in *n-p* cross section measurements;

(2) a total cross-section measurement at 0.4926 MeV to an accuracy of $\pm 0.18\%$ (The purpose of this particular measurement is twofold. First, to determine the best possible value of the neutron-proton singlet effective range for testing charge independence; second to set a base line for measuring shape dependence deviations.);

(3) a preliminary total cross-section measurement at 3.205 MeV to an accuracy of $\pm 0.31\%$, obtained from data taken to investigate rate dependence effects.

II. REDUCTION OF UNCERTAINTIES IN PRECISION CROSS-SECTION MEASUREMENTS

A. Important Uncertainties

Hafner *et al.*[8] list eight factors which contribute uncertainties of between 0.1 and 0.2% to their *n-p* cross-section measurement at 4.75 MeV (net error 0.39%). In order to achieve the desired precision in the present experiment it was necessary to reduce substantially each of these uncertainties. The factors are listed below in a sequence convenient for this discussion.

(1) Background neutrons and gamma rays from walls of the room.

(2) Background neutrons and gamma rays which are produced at or near target and which travel through the transmission sample to counter.

(3) Neutrons detected in the counter after being multiply scattered in the transmission sample.

(4) Counting statistics. (a) Note that the solid angle subtended by the detector at the sample was limited by the need to keep uncertainty 3 small. (b) Note that the transmissions used were much higher than that which would be optimum if uncertainty number one were negligible.

(5) Neutron energy uncertainty.

(6) Rate dependent errors.

(7) Determination of the number of hydrogen atoms per cm^2.

(8) Misalignment.

B. Reduction of Uncertainties Because of Resonant Detectors

A new feature of the present measurements is the use of resonant reactions of narrow width for neutron detection, which makes it possible to reduce greatly

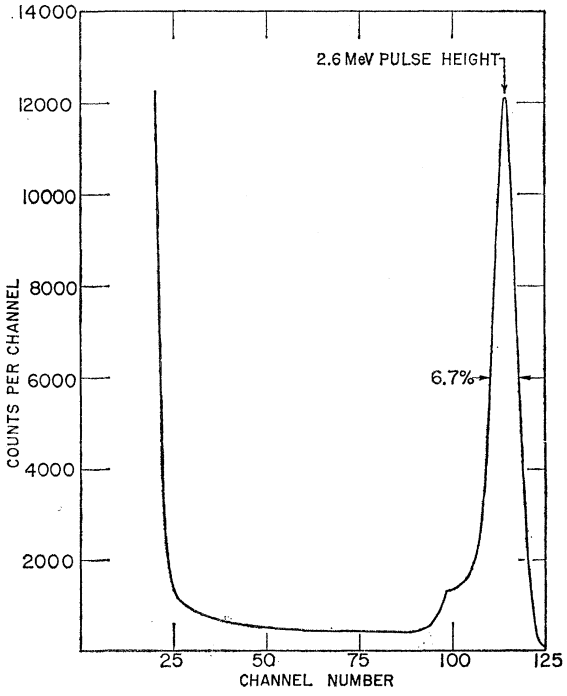

FIG. 4. Pulse-height spectrum caused by 3.2-MeV neutrons on a gas scintillation counter filled to 250 psi neon plus 50 psi xenon. The peak is due to alpha particles from the $Ne^{20}(n,\alpha)O^{17}$ reaction which are stopped in the active volume.

the first five of the uncertainties listed above. All previous precision total n-p cross-section measurements were done with counters which detected neutrons by the recoil of protons or He^4 nuclei from the elastic scattering of neutrons. Such detectors have appreciable sensitivity to neutrons of different energy than the primary beam, the major sources of errors 1, 2, and 3. With a sharply resonant neutron detector these sources of error can be reduced by a factor nearly as great as the ratio of the resonance cross section to the off resonance cross section.

A very important advantage of resonant detection in n-p scattering is that the uncertainty in neutron energy can be greatly reduced, since the resonance peak furnishes an energy at which to operate which is reproducible to several percent of the resonance width. Furthermore, a change in the energy of the incident neutrons results in only half as great a change in the effective energy of the neutrons detected when the target thickness is comparable to the resonance width. For the resonances used in the present work, the effective neutron energy can be reproduced to $\pm 0.03\%$. This figure is also the minimum uncertainty in the energy which might be obtained if a perfectly accurate absolute measurement were made of the resonance energy.

In addition, a resonant detector offers a unique method for taking backgrounds by shifting operating energy, which makes it possible to measure even those backgrounds which are due to other interactions in the neutron producing target.

The reduction in sensitivity to neutrons entering the detector after multiple scattering makes it possible to increase the solid angle the detector subtends at the sample and obtain a greater counting rate with a detector of a given efficiency. When the solid angle is increased by bringing the detector closer to the source, the signal to background ratio is improved, allowing shielding to be omitted. Due to the reduction of the background and multiple inscattering uncertainties, an optimum transmission for the sample can be selected to give the most accurate value of the cross section in a specific running time.

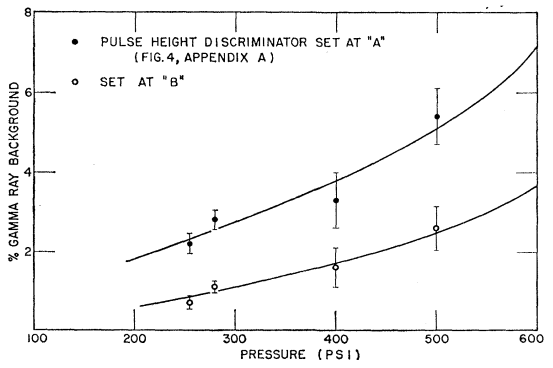

FIG. 5. Dependence of percentage background on total gas pressure of a 20% N_2 80% xenon mixture detecting 0.5-MeV neutrons. The background was obtained by shifting bombarding energy 80 keV below that required to excite the resonance.

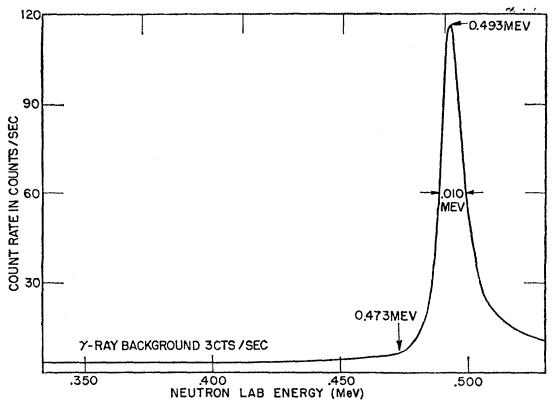

FIG. 6. Count rate vs incident neutron energy for scintillator filled to 100 psi N_2 plus 400 psi xenon.

Finally, the single inscattering correction is greatly reduced because the neutron loses sufficient energy when scattered by a proton that the detection efficiency is greatly reduced. In a geometry in which a "flat" detector would require a correction of 4%, the resonant detector may require only a 1% correction. However, a complication is introduced as the calculation of this correction for a resonant detector requires an accurate knowledge of the resonance width and the target thickness and thus introduces an uncertainty which is not present for a flat detector. The correction has been expressed as a sevenfold integral and calculated by numerical integration on an IBM 650 computer. (See Appendix.)

After an investigation of the available experimental (n,p) and (n,α) cross-section data the resonance in the $N^{14}(n,p)C^{14}$ cross section at 0.4926-MeV neutron energy was chosen for the measurement near 0.4 MeV needed to determine the singlet effective range. Resonances in the $Ne^{20}(n,\alpha)$ cross section at 3.2, 5.9, and 7.5 MeV are available for those measurements needed to determine shape dependent deviations.

A high-pressure gas scintillator was developed utilizing nitrogen-xenon, and neon-xenon gas mixtures at pressures up to 1200 psia.[13] Figures 3 and 4 show the pulse-height spectra obtained when detecting neutrons in these gas mixtures. The detection efficiency of the nitrogen-xenon scintillator is limited to about 0.05% by the poisoning action of the nitrogen and the increase of gamma-ray backgrounds with absolute pressure shown in Fig. 5. The neon-xenon detector can achieve efficiencies greater than 1%. Figure 6 shows how the count rate of the nitrogen-xenon scintillator varies with the energy of the incident neutrons. The curve is essentially a plot of neutron detection efficiency versus neutron energy, distorted slightly by the change in

[13] C. Engelke, I.R.E. Trans. Nucl. Sci. 7, 32 (1960).

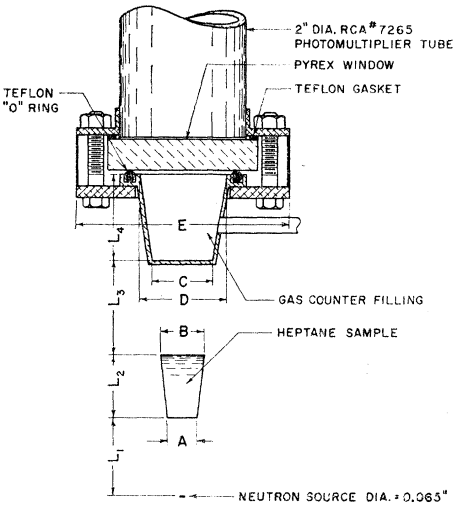

FIG. 7. Schematic diagram of neutron source, sample, and detector geometry. The lettered dimensions for different runs are given in the text.

yield of the Li(p,n) reactions as the proton energy is varied. This resonance is an especially favorable resonance, having a peak to off resonance ratio of at least 100 to 1. However, within the present limitations on accuracy imposed by the remaining uncertainties, the use of resonances detectors is almost equally valuable for ratios of as little as 4 to 1.

C. Reduction of Other Uncertainties

Count rate dependence uncertainties were reduced to a negligible level by performing auxiliary measurements of transmission versus count rate at rates an order of magnitude larger than those employed in the precision experiment.

In order that the C—H ratio be known accurately, a stochiometric compound, n-heptane, (C_7H_{16}) was employed as a transmission sample. A vapor chromatography analysis showed the heptane used in our measurements to be pure to 0.1%.

For both flat and resonant detectors the single inscattering correction and multiple inscattering uncertainty increase with the solid angle subtended by the detector at the scatterer. Therefore, the scatterer was placed as close as feasible to the source to give the smallest inscattering correction at the given detector to neutron source distance.[14]

In the present experiment the source to detector distances were chosen so that the solid angle subtended at the detector resulted in about equal values for the uncertainty in counting statistics and the uncertainty in the inscattering correction. The sizes of the two detection volumes were fixed to give the best pulse-height resolution when used with 2- and 3-in. photomultiplier tubes, respectively. A better optimization of the source to detector distance could have been made if the detector dimensions could have been made to an arbitrary scale without loss of pulse-height resolution.

Neutron source dimensions and alignment uncertainties were pared to the minimum, so that the scatterer and detector volumes did not vary greatly from the cone frustums which ideal point source geometry requires. The scatterer's diameter was sufficiently large so that no misalignment error was introduced even for the maximum deviation in position tolerated by the alignment procedure.

III. CROSS-SECTION MEASUREMENTS AT 0.4926 AND 3.200 MeV

A. Experimental Methods

1. Neutron Source

The intensity of the neutron source was an important factor in the 0.4926-MeV cross-section measurement. Pure lithium metal targets were found to be unsuitable because the effective target thickness increased too rapidly during bombardment, due to lithium's chemical reactivity. The lithium compound having the best yield per unit stopping power is lithium hydride. LiH targets, 5 to 10 keV thick at threshold were evaporated and proved stable under bombardment for 4 to 8 h at a proton current density of 10 μa/mm^2. The use of relatively thick target backings of high thermal conductivity was also an important factor in permitting stability under these high current densities. The carbon buildup on the target was reduced by a factor of nearly 100 by use of a re-entrant liquid-nitrogen trap which subtended a solid angle of approximately 2π at the target spot. The neutron source was confined to an area of 0.065-in. diameter by a 0.060-in. gold collimator placed a distance of 4 in. from the target. It was possible to pass 90% of the beam current through this collimator by using an electrostatic quadrupole lens of variable astigmatism to focus the beam. For the 3.205-MeV transmission measurements a LiH target was used which had a stopping power of 38 keV for the 4.87-MeV protons required to produce 3.2-MeV neutrons.

The forward-direction neutron flux was employed throughout all measurements, the center of the detector being placed at 0°.

2. Detection Equipment and Geometry

The nitrogen-xenon and neon-xenon gas scintillation counters previously discussed were viewed with an RCA type 7265 photomultiplier tube which was especially selected by RCA for high photocathode

[14] Earlier workers, in minimizing an expression for the single inscattering correction, kept the scatterer diameter fixed in differentiating with respect to the source to scatterer distance, coming to the erroneous conclusion that the scatterer should be placed halfway between the source and detector. However, for a beam diverging from a point source the scatterer diameter required to shadow a given detector is proportional to the source to scatterer distance.

TABLE II. Values of the dimensions (in inches) shown in Fig. 8 for the three scattering geometries employed.

	A	B	C	D	E	L_1	L_2	L_3	L_4
					At 0.4926 MeV				
(a)	0.475	0.705	0.97	1.37	3.00	1.40	0.9989	1.75	1.40
(b)	0.350	0.925	0.97	1.37	3.00	1.05	1.995	1.25	1.40
					At 3.205 MeV				
	0.350	0.925	1.96	2.88	4.00	1.05	1.995	5.50	4.00

sensitivity. Amplified pulses were fed into two scalers and a 256-channel analyzer.

Figure 7 and Table II show all the relevant dimensions for this and two other scattering geometries employed. For these geometries the sensitive volume of the scintillator remains in the umbra of the sample for all points on the 0.065-in.-diam source even if radial alignment errors as large as 0.035 in. are made. The walls of the counter volume are in the umbra of the sample as long as alignment errors are less than 0.020 in.

The establishment of a common axis for the beam, sample holders and counters was achieved with the aid of a spot created by the beam on a glass window near the plane of the sample holder. The line traversed by the beam was established by observing the spot and the collimator hole through a telescope having an aperture of $\frac{1}{4}$ in., placed at a distance of 30 in. from the window. A fiducial mark on the scatterer was then brought onto the line thus established.

Normal radial alignment accuracies were ± 0.008 in. in the position of the front end of the sample holder. This figure combines an uncertainty of ± 0.006 in. in setting the position and an uncertainty of ± 0.005 in. due to the observed reproducibility of the remote control sample changing apparatus. The positions were monitored hourly with a cathetometer and were rechecked by repeating the alignment procedure at the end of each run. The axis of the sample blank and detector were set parallel to the beam axis to within ± 0.005 rad by observing from a point on the beam axis a perpendicular light reflection from a mirror mounted on the flat surface of each frustum.

On only one occasion did an abnormally large misalignment occur. The routine check at the end of the transmission run on the 2-in. scatterer at 0.4926 MeV revealed a radial misalignment of 0.025 in. This left one section of the brass counter wall unshadowed by the sample for a small sector of the beam spot. A conservative estimate of the error introduced by unattenuated neutrons scattering into the counter from this wall gave an upper limit of 0.01% to the error in cross section. Therefore, no correction was needed even for this unusually bad alignment.

In the two geometries used at 0.4926 MeV a large section of the counter flanges is deliberately left out of the umbra of the sample. The uncertainties introduced by this procedure are small because the off-resonance detector efficiency is low. This small uncertainty was preferable to the increase in the uncertainty in the inscattering correction which would have occurred if the sample size had been large enough to keep these flanges in the umbra. These flanges were made of the minimum thickness of aluminum consistent with the necessary mechanical strength. In the geometry of the 3.205-MeV measurement all counter parts are included in the umbra. The scatterer positions used for both the 0.4926- and 3.205-MeV mesaurements do not minimize the inscattering correction for the detector sizes and positions chosen. However, the minimum value cannot be more than 10% lower than the actual values. The determination of the exact optimum scatterer positions would have required a large amount of numerical computation, and the small improvement that would be obtained did not justify the magnitude of the calculation.

3. *Procedure*

The transmissions of two liquid n-heptane samples 1 in. and 2 in. thick, respectively, were measured relative to carbon blanks which had approximately the same number of carbon atoms per square centimeter as the heptane samples. The relative transmissions at 0.4926 MeV were about 0.37 and 0.13, respectively. The samples and blanks were held by hollow stainless steel cone frustums machined out of solid stock with a wall thickness of 0.015 in.

The neutron flux was monitored by integrating the proton beam current. The alternative procedure of monitoring the neutron flux directly was not employed in order to avoid the complication of the sample scattering neutrons into the neutron monitor. At 0.4926 MeV four independent measurements were made, each with a statistical accuracy of about $\pm 0.16\%$, three using the 1-in. sample, and one using the 2-in. sample. Each measurement required approximately 100 h of data taking. The neutron energy spreads for the different measurements were 7, 9, and 11 keV for the thin-sample measurements, and 7 keV for the thick-sample measurement. The gamma-ray backgrounds varied between 1 and 8% of the blank counting rate, which was between 20 and 100 counts/sec. Two pulse-height intervals were used in measuring each transmission. The respective intervals included all pulses above the heights marked A and B in the pulse-height spectrum of Fig. 4. All measured values of the cross section agreed within statistical fluctuations. No significant correlation in deviations from the norm with transmission, relative background, count rate, or target thickness was observed.

At 3.205 MeV the transmission of the 2-in. heptane sample was measured using several different counting rates in order to obtain the correction for counting rate dependence on the measurement at 0.4926 MeV. The detector filling consisted of 425 psia neon and 75 psia xenon. The sample transmission, which was about

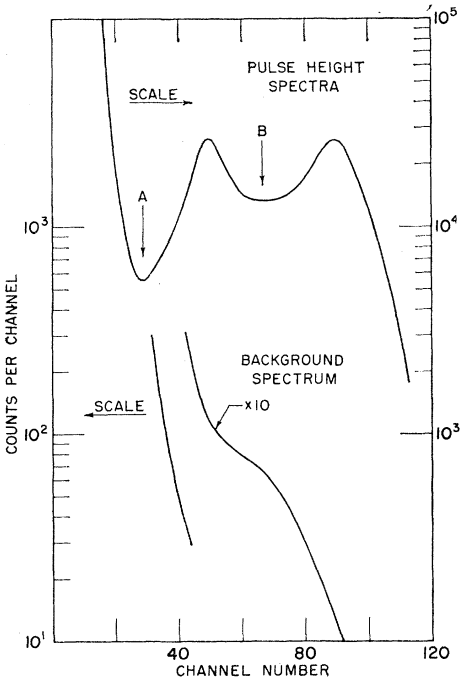

FIG. 8. Pulse-height spectra caused by 3.2-MeV neutrons incident on a gas scintillator filled to 425 psi neon plus 75 psi xenon. The double peak is due to differing light collection from different regions of the scintillator active volume as a result of insufficient wall reflectivity.

0.48, was measured with a statistical standard deviation of $\pm 0.08\%$ at count rates of 700, 1700, and 2300 counts/sec.

In taking the rate-dependence data an effort was made to obtain a pulse-height spectrum resembling that given by the nitrogen-xenon detector at 0.4926 MeV. By using a thinner reflective coating of magnesium oxide on the walls of the scintillator it was found possible to distort the spectrum obtained under optimum conditions from the neon (n,α) reaction at 3.205 MeV (Fig. 4) into the spectrum shown in Fig. 8.[15] As before, two pulse-height intervals were used in measuring the transmission, including all pulses above the height marked A or B in Fig. 8. The photomultiplier's voltage was adjusted to give the same pulse height at the last stage of the photomultiplier tube as in the 0.4926-MeV measurements. Thus, the rate-dependence measurements were performed with similar pulse-height distributions as well as identical electronic equipment. Figure 9 shows the observed dependence of transmission on count rate.

As a by-product of the count-rate dependence check, a value of the n-p cross section at 3.205 MeV has been obtained, but not with the ultimate accuracy of which the method is capable. Even so, the uncertainty in this relatively crude measurement is less than that for any previous measurement. Further measurements at this energy are now in progress.

The apportionment of time between sample-in, sample-out signal and background was kept as close as convenient to those optimum apportionments given by Rose.[16] Signal and background runs were alternated continuously over a 24-h running day to minimize the effects of drifts. Between signal runs the resonance energy was relocated to $\pm 0.03\%$. Signal runs were of from 1 to 2 h duration; the sample was cycled in and out at intervals of the order of 5 min by means of a servo-motor gear system which moved a sliding "window" in which the sample and blank were mounted.

"Sample in" and "blank in" pulse-height distribution were stored separately in two halves of the 256-channel pulse-height analyzer. The spectrum from each signal and background run at 0.4926 MeV was printed out and inspected for gain drifts. However, such drifts introduced errors only when the background runs were not symmetrically spaced in time about the signal run. In these instances the time-varying background was interpolated to the value which it had at the time the signal run was performed.

The transmission at 0.4926 MeV was calculated from the following equation:

$$T=\frac{N_{\text{in}}-N_{\text{in}}(E-20\text{ keV})}{N_{\text{blank}}-N_{\text{blank}}(E-20\text{ keV})}, \tag{4}$$

where N_{in} is the counting rate with the sample in the beam at the resonant energy of the detector, $N_{\text{in}}(E-20$ keV) is the counting rate with the sample in the beam but the energy of the beam is 20 keV below the energy of resonance detection, N_{blank} is the counting rate with the carbon blank in the beam at the resonant energy of the detector, and $N_{\text{blank}}(E-20$ keV) is the counting rate with the carbon blank in the beam but the beam

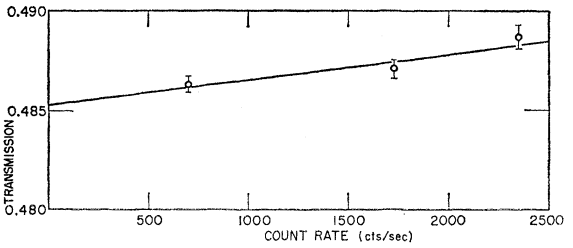

FIG. 9. Experimental dependence of a transmission on counting rate at rates up to 20 times those normally used.

[15] The contrast between Fig. 4 and Fig. 8 illustrates the importance of wall reflectivity in gas scintillators. For good pulse-height resolution when detection occurs over an extended volume it is necessary to use MgO coatings much thicker than those which seem perfectly white by visual inspection. It is also important to make the ratio of window area to wall area as large as possible. The two peaks which appear in Fig. 8 are caused by geometric effects. The use of a collimated neutron beam shows that the larger pulses come from the end of the counter near the window, while the smaller pulses come from the end furthest from the window.

[16] M. E. Rose and M. M. Shapiro, Phys. Rev. 74, 1853 (1948).

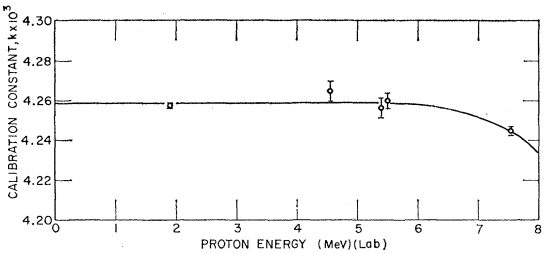

FIG. 10. Magnetic analyzer calibration constant as a function of equivalent proton energy. $E_p=kf^2(1-kf^2/2mc^2)$ where f is the Numar frequency in megacycles per second and E_p is in MeV.

energy is 20 keV below the resonant energy of the detector.

4. *Energy Measurements*

All transmission runs were performed at the machine energy which produced the maximum counting rate on the resonance curve observed with the blank in place. If the target material is uniform and a detector of conical shape is used in the forward direction and the resonance is symmetrical and isolated, the average neutron energy will be equal to the resonance energy when the maximum counting rate is obtained. As the $N^{14}(n,p)$ resonance at 0.4926 MeV is symmetrical and well isolated, the effective neutron energy at which it was measured is equal to the resonance energy. The determination of the absolute energy of the $N^{14}(n,p)$ resonance can be reduced to the determination of the difference between 2 proton energies which are about 350 keV apart. The 90° magnetic analyzer associated with the Columbia University Van de Graaff accelerator is well suited to this task. The analyzer's magnetic field is measured by an observation of the proton magnetic resonance frequency. It is used as a relative instrument and calibrated by observing nuclear reactions of known energy. The frequencies corresponding to the $Li^7(p,n)$ threshold, and to the higher proton energy for which $Li^7(p,n)$ neutrons are at the $N^{14}(n,p)$ resonance energy, have been determined with three different lithium target thicknesses to $\pm 0.005\%$ for each target.

The magnetic analyzer calibration constant is a slowly varying monotonic function of energy which changes by $0\pm 0.01\%$ between the two energies in question (See Fig. 10). The known absolute lithium threshold energy[17] gives the calibration constant at threshold to $\pm 0.02\%$.

The apparent resonance energy must be corrected by subtracting one half the neutron energy spread. The lithium target thicknesses were found to be 2, 5, and 10 keV$\pm 20\%$ from analysis of the yield curves just above the $Li(p,n)$ threshold. The three resonance energy measurements were 0.4926 ± 0.0006, 0.4924 ± 0.0007, and 0.4934 ± 0.0011 MeV.

[17] J. B. Marion, Revs. Mod. Phys. 33, 139 (1961).

The uncertainty in our operating energy is greater than the uncertainty in the resonance energy because of two factors. First, the relocation of the resonance for each signal run introduces an uncertainty of ± 0.15 keV. Second, nonuniformity of the target can cause the effective energy to vary from the resonance energy when operating at maximum count rate. An allowance of ± 0.3 keV is made for this effect. The net uncertainty in the effective neutron energy is ± 0.65 keV corresponding to an uncertainty in cross section of $\pm 0.067\%$.

The energy of the protons required to produce $Li^7(p,n)$ neutrons at the $Ne^{20}(n,p)$ resonance near 3.2 MeV was located relative to our magnetic analyzer scale to ± 0.6 keV. The present uncertainty in the absolute value of this resonance energy is mainly due to the uncertainty in the absolute energy of the calibration points used. The value of the magnetic analyzer calibration constant versus energy was measured by repeated observations of the $Li^7(p,n)$ threshold and several $F^{19}(p,\gamma)$ resonances using both a proton beam and an HH^+ beam. Figure 10 shows these data. The value of the resonance energy is found to be 3.200 ± 0.006 MeV. As there is a nearby resonance which distorts the symmetry of the cross-section curve, the effective operating energy is taken as $E=3.205\pm 0.006$ MeV. The corresponding uncertainty in the value of the cross section due to the uncertainty in the absolute energy at which the cross section is actually measured is $\pm 0.13\%$.

B. Corrections

1. *Correction for Neutrons Inscattered by Sample*

Due to the sensitive dependence of the detection cross section on neutron energy, the calculation of the number of inscattered neutrons detected required a seven-dimensional integration over three scatterer coordinates, three detector coordinates, and one energy parameter.

In setting up the calculation, account was taken of the variation of neutron energy with the depth in the target at which the neutrons are produced, with the angle at which the neutrons leave the target, and with the angle by which the inscattered neutrons are scattered by the hydrogenous sample. The dependence of the scattering amplitude of hydrogen on the scattering angle was also taken into account, as was the attenuation of the direct and inscattered neutron flux in passing through the sample or the carbon blank. The neutron detection cross section was taken as the single-level Breit-Wigner formula. The variation of entrance channel width with incident neutron energy was included while the variation of exit channel width was ignored because its importance did not warrant the inclusion of its awkward functional form. The neglect of exit channel width variation introduces an error of less than 1% of the inscattering correction in the present

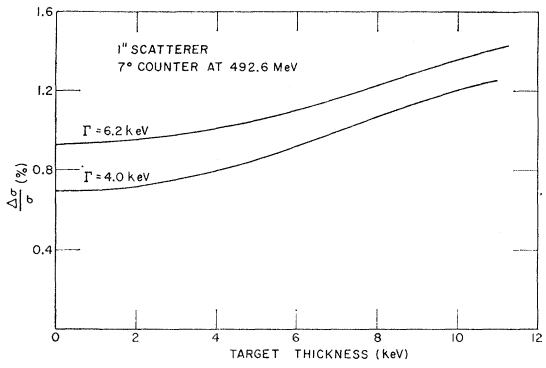

FIG. 11. Calculated inscattering correction vs target thickness for geometry of 0.4926-MeV measurements, 1-in.-long sample, and assuming two different resonant widths for the $N^{14}(n,p)C^{14}$ reaction.

work. Note that if it were desired to make this calculation for a negative-Q reaction not far above threshold, the exit channel width variation would have to be included. Other factors neglected were: neutron yield variation with angle of production, neutron attenuation in the gas scintillator, and the increase in attenuation of scattered neutrons in the sample due to longer path and lower energy. In assessing the accuracy of these approximations it should be remembered that the energy region of importance in the integration is confined to vicinity of the resonance.

The correction to the cross section depends on the ratio of the number of inscattered neutrons detected to the total number detected. The number of neutrons detected directly was set up as a four-dimensional integration over the detector coordinates and an energy parameter, using the same approximations as in calculating the number inscattered. The four-dimensional integral was performed analytically after some minor approximations, while it was found necessary to employ an IBM 650 computer in evaluating the seven-dimensional integral. Further discussions of the inscattering correction is made in the Appendix of this paper. Figure 11 gives a plot of the calculated correction versus target thickness for two hypothetical values of the resonance width. These curves apply to the geometry used with the 1-in. sample holder at 0.4926 MeV, and assume a $Li(p,n)$ neutron source. The value of this correction ranged between $0.9\pm0.09\%$ and 1.3% $\pm0.11\%$ for the various conditions set up in the four runs at 0.4926 MeV. For the 3.205-MeV measurements it was also necessary to estimate the contribution of other resonance in the $Ne^{20}(n,\alpha)$ reaction. The total correction to the measured cross section at 3.205 MeV was $+1.1\pm0.20\%$. The major sources of uncertainty in these corrections are the experimental measurements of target thickness, resonance width, and operating energy. A conservative allowance of $\pm5\%$ of the correction is made for possible error in the numerical integration. Target thicknesses were estimated from the observed dependence of neutron yield on energy just above the $Li(p,n)$ threshold. The resonance widths were found in two ways, first from the width of thin-target yield curves and second, from plots of the type shown in Fig. 12. The quantity $[(\sigma_0/\sigma)(E_{res}/E)^{1/2}-1]$ is plotted versus $(\Delta E)^2$ for $N^{14}(n,p)$ resonance at 0.4926 MeV. The linearity of this plot is evidence that the single-level Breit-Wigner formula is applicable over the energy range important in the integration, while the slope of this line gives an accurate value of Γ^2.

2. *Correction for Count Rate Dependence*

Assuming a linear fit to the experimental rate dependence data the correction to the cross section at 0.4926 MeV is taken as $+0.02\pm0.01\%$. By extrapolating the rate-dependence data to zero rate, a cross-section value at 3.205 MeV was found with an uncertainty of $\pm0.10\%$ due to the extrapolation.

3. *Correction to Background Subtraction Method*

The expression used to calculate T [Eq. (4)] would give the desired transmission at the resonance energy were it not for two minor effects. First, the gamma-ray background may change slightly between energies, due to the 0.9% increase in proton bombarding energy. By observing the portion of the scintillator pulse-height spectrum below the neutron peak this change was found to be an increase of $3.4\pm0.3\%$ over the pulse-height range from 0.3 to 0.7 MeV. This change requires a correction to the cross section of the order of 0.1 $\pm0.01\%$ for some of the data. The second correction which is necessary occurs because the detector efficiency is not actually zero for the lower energy neutrons which strike the detector at the background energies and have a different transmission in the sample. The calculated correction on the measured cross section is $+0.02$ $\pm0.01\%$.

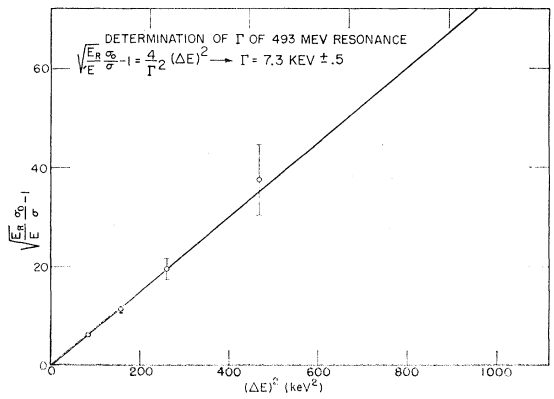

FIG. 12. Determination of width of the $N^{14}(n,p)C^{14}$ resonance at 0.4926 MeV.

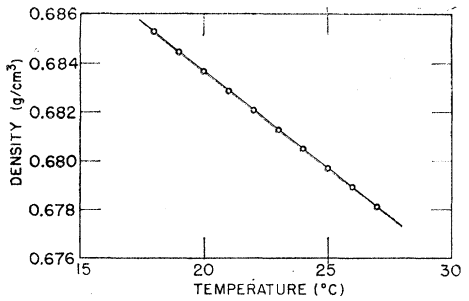

FIG. 13. Density of heptane vs temperature as measured for this experiment.

4. *Correction for Beam Contamination by Neutrons of Different Energy*

No correction was necessary for off-resonant neutrons in the 0.4926-MeV measurement; however, in the 3.205-MeV measurement a second group of neutrons from the $Li^7(p,n)Be^{7*}$ reaction contributed counts. The relative intensity of the neutron groups which leave Be^7 in its ground and first excited states was measured with a proton recoil counter telescope.[18] The intensity for the first excited state group at $E=4.9$ MeV and 0° was found to be $9\pm1\%$ of the neutron intensity which results from the transition to the ground state of Be^7. The ratio of the $Ne^{20}(n,\alpha)$ counting rate at the resonance energy to that obtained by shifting the machine energy to cause the ground-state group to lie 430 keV below the resonance energy was measured as 10 to 1 (where 430 keV is the excitation energy of the first excited state above the Be^7 ground state). Since the target was the same as that used for the cross-section measurement, this ratio gives the relative sensitivity of the detector for the two neutron groups when operating at the resonance energy. A small correction is necessary for the change with energy of yield in neutrons for the ground-state transition and the contribution from the low-energy group at the reduced energy. The fraction of the detected neutrons which have the lower energy is thus $0.9\pm0.1\%$. The measured T is thus $0.991T$(3.2 MeV)$+0.009T$(2.77 MeV). The necessary cross-section correction is $-0.09\pm0.01\%$ since the n-p cross section is greater by 10% at the lower energy.

5. *Correction for the Variation of Heptane Density with Temperature*

The relative density of heptane was monitored directly to $\pm0.01\%$ by observing the height of the liquid in a vertical capillary tube affixed to the sample holder. An uncertainty of $\pm0.05\%$ in the heptane density is derived mainly from the fluctuations in the values measured at hourly intervals. Figure 13 shows measurements made with a pycnometer of the absolute heptane density versus temperature. The data agree within 0.02% with the value given in the handbook of Chemistry and Physics. The liquid level gauge was used as a relative instrument, and was calibrated against the same thermometer used in the absolute density measurements. Therefore, no uncertainty due to thermometer accuracy was introduced.

An additional correction is necessary for each run as the graphite blank gives a perfect carbon subtraction at only one density. The correction for this effect was about $+0.1\%$ in cross section for all of the runs. The only important source of uncertainty in this correction is in the determination of the density of the specific graphite sample. An accuracy of $\pm0.1\%$ in these density measurements produced an uncertainty of $\pm0.02\%$ on the measured cross section.

6. *Calculation of Effective Length of Transmission Sample*

In the close geometry used in our experiment the variation of transmission with the angle at which the neutron traverses the sample cannot be neglected. The average value of the transmission is

$$\bar{T}=\int_0^{\theta_{\max}}\exp(-kl_0/\cos\theta)\sin\theta d\theta \Big/ \int_0^{\theta_{\max}}\sin\theta d\theta$$

$$\cong\exp(-kl_0)\int_0^{\theta_{\max}}(1-kl_0\theta^2/2)(\theta-\tfrac{1}{6}\theta^3)d\theta \Big/ \int_0^{\theta_{\max}}(\theta-\tfrac{1}{6}\theta^3)d\theta, \quad (5)$$

$$\bar{T}\cong[\exp(-kl_0)](1-kl_0\theta_m{}^2/4)$$

$$\cong\exp[-kl_0(1+\theta_m{}^2/4)]. \quad (6)$$

Thus, this correction can be made by using an effective average value of l equal to $l_0(1+\theta_m{}^2/4)$. For the geometries used at 0.4926 and 3.205 MeV, $(1+\theta_m{}^2/4)$ is equal to 1.0039 and 1.0033, respectively. The inclusion of all terms up to the order of θ^4 in the expansions showed that the use of the above expression introduced cross-section errors less than 2 parts per 100 000.

7. *Correction for Difference in End Wall Thicknesses of Sample Container and Blank Container*

The average wall thicknesses were measured to an accuracy of ±0.0002 in. using a micrometer with a small probe. The 1-in. sample container had a wall thickness less by 0.0014 ± 0.0002 in. than the 1-in. blank container. The resulting difference in the transmissions of the empty containers required a correction of $+0.09\pm0.02\%$ to the experimental cross section at 0.4926 MeV. The 2-in. sample holder had a wall thickness greater by 0.0043 ± 0.0003 in than the 2-in. blank holder. The required correction was $-0.19\pm0.02\%$ at 0.4926 MeV and $-0.40\pm0.05\%$ at 3.205 MeV.

[18] R. E. Benenson, Rev. Sci. Instr. 29, 1 (1958).

TABLE III. Uncertainties in the measured cross section due to various experimental factors.

	At 0.4926 MeV	At 3.205 MeV
(1) Counting statistics	±0.095%	±0.15%
(2) Neutron energy uncertainty	±0.067%	±0.13%
(3) Inscattering correction uncertainty	±0.101%	±0.20%
(4) Length of sample uncertainty	±0.05%	±0.03%
(5) Heptane average density uncertainty	±0.05%	±0.05%
(6) Graphite blank density uncertainty	±0.02%	±0.02%
(7) Gamma-ray background uncertainty	±0.02%	±0.00%
(8) Neutron background uncertainty	±0.02%	±0.03%
(9) Heptane purity uncertainty	±0.01%	±0.01%
(10) Rate dependence uncertainty	±0.01%	±0.10%
(11) Multiple inscattering uncertainty	±0.005%	±0.10%
(12) Uncertainty due to measurement of difference in end wall thickness of sample holder and blank holder	±0.02%	±0.05%
Net uncertainty	±0.18%	±0.31%

8. Correction for Neutrons Inscattered by Unshadowed Matter

For the measurement at 0.4926 MeV the required correction was calculated as $+0.03\pm0.02\%$. This differs from zero only because the counter flanges were deliberately left out of the shadow volume in the measurements at 0.4926 MeV as discussed in Sec. IIIA. For the data at 3.205 MeV the correction was measured directly, using a "thick" Lucite scatterer to filter out the direct beam. The spectra of this background is shown below the signal spectrum in Fig. 8. For the upper discriminator setting the correction was $+0.07\pm0.03\%$, for the lower setting the correction was $+0.5\pm0.25\%$. Only the data using the high discriminator setting were used in calculating the cross-section value at 3.205 MeV. The relatively large values of these corrections are caused by the very poor pulse-height resolution deliberately produced. Future measurements will employ distributions like that of Fig. 4.

9. Correction for the Scattering of Neutrons by Air

This correction was $+0.03\%$ for the 0.4926-MeV measurement and $+0.06\%$ for the 3.205-MeV measurement.

C. Experimental Uncertainties

Table III summarizes the contributions of various experimental factors to the uncertainty in the measured cross sections. The net uncertainty is taken as the square root of the sum of the squares of these factors.

Preliminary to determining the uncertainty due to counting statistics, the four runs at 0.4926 MeV were subjected to and passed a χ^2 test. Each run contained about 16 independent measurements. The data used at 3.205 MeV contained 5 independent measurements and also passed a χ^2 test. The quoted cross sections result from weighted averages of all results. The uncertainties listed are calculated root mean square deviations, assuming Gaussian distributions for signal and background fluctuations. All the other uncertainties in Table III have previously been discussed.

IV. CONCLUSIONS

A. The cross-section measurement of $\sigma=6.202\pm0.18\%$ at 0.4926 MeV determines the (n,p) singlet effective range to be 2.46 ± 0.12 F. This value is to be compared with $r_{0s}=2.75\pm0.21$ F, obtained from the data of Fields *et al.*[9] at 1.0 MeV, using the most recent values of a_c and ϵ_d. A conservative upper limit to a systematic error in the present measurement which could be introduced by shape-dependent effects is ±0.04 F.

B. The measurement at 3.205 MeV, $\sigma=2.206\pm0.31\%$, indicates a shape-dependent deviation of $+0.32\%$ from the base line established by the 0.4926-MeV measurement, as shown in Fig. 15. This trend, although not yet significant, favors a negative triplet n-p shape parameter such as is obtained from a Yukawa well with a repulsive core.

V. DISCUSSION

A. To obtain values of both the depth and range of the two-body interaction, both the scattering length and the effective range must be utilized. The improvement in accuracy achieved in the present measurement of the n-p singlet effective range will therefore be reflected in comparable improvements in our knowledge of both the strength and the range of the n-p singlet interaction as the accuracy of the singlet effective range is at present the limiting factor.

An important aspect of this improvement in our knowledge of the n-p singlet system is its bearing on the controversial issue of charge dependence of nuclear forces. The conclusion previously drawn from the comparison of the p-p and n-p singlet scattering amplitudes taken alone was that if the ranges of the n-p singlet and p-p interactions are equal, the depth of the n-p interaction is 3% greater than that of the p-p interaction.[19] Another sensitive means of detecting deviations from charge independence is the comparison of the energies of isobaric triplet energy levels. This comparison has yielded the result that the n-p interaction energy is 1% greater than the p-p interaction energy.[20] However, this method requires the assumption of charge symmetry and is an order of magnitude more sensitive to charge symmetry deviations than to charge independence deviations.

The comparison which would be appropriate here, of the range and depth of n-p singlet and p-p interaction is prevented by the fact that the p-p effective range, although quite precise, is subject to large systematic shape dependent uncertainties. Depending on the shape

[19] Riazuddin, Nucl. Phys. **7**, 217 (1958).
[20] D. H. Wilkinson, Phil. Mag. **1**, 1031 (1956).

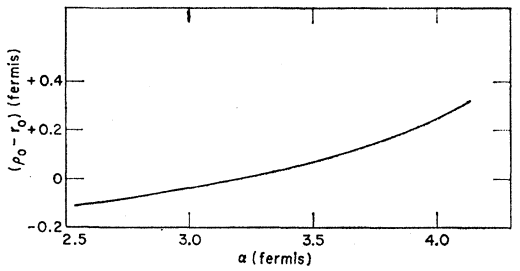

FIG. 14. Correction to p-p effective range as function of radius α at which nuclear forces becomes small compared to Coulomb forces.

parameter assumed in analysis, Hall and Powell[21] quote values of 2.79 F for $P=+0.055$ (simple Yukawa potential) and 2.57 for $P=-0.03$ (square well).[22] Furthermore, the p-p effective range integral is not identical to that appearing in the n-p theory, as the wave functions involved are solutions for nuclear plus electrostatic potentials rather than nuclear potentials alone.

Sachs[23] presents an approximate expression for calculating this difference:

$$\rho_0 - r_0 \cong 2\int_0^{\alpha} (V_c^2 - V_n^2)dr,$$

where ρ_0 is the apparent p-p effective range, r_0 is the corrected p-p effective range for comparison to the n-p range, α is radius at which nuclear forces become small compared to electrostatic forces, a_{singlet} is the n-p singlet scattering length, $V_N=(1-r/a_{\text{singlet}})$, $V_C=[1+(r/28.8)\ln 1.74r]$, and all lengths are in fermis.

Figure 14 is a plot of this correction versus α. The proper value of α is only well defined for a square well with $\alpha=\rho_0\cong 2.65$ and for which the correction is -0.10 F. For long-tailed potentials the correction becomes positive and is fairly large. However, a better method of calculation is required to give the correction for realistic potentials and it is hoped that this paper will generate interest in this correction.

Fortunately an analysis of the latest p-p scattering results is now in progress[24] and is expected to yield a more accurate value of the p-p effective range together with an experimental p-p shape parameter. This effective range value, along with an accurate evaluation of the correction discussed by Sachs, would allow separate checks on the charge independence of the depth and of the range of two-body interactions.

B. Figure 15 compares the deviations of experimental cross-section measurements from the shape-independent approximation with those predicted for some particular values of the parameters P_t and P_s. As the singlet and triplet potentials are known to differ in shape, P_t and P_s may have opposite algebraic signs and a monotonic increase of shape-dependence effect with energy is possible, as shown by curves 1 and 4 of Fig. 15(b).

Throughout this paper the value of k^2 used in Eq. (1) for calculating cross-section values has been:

$$k^2=1.2049\ E_{\text{lab}}\times 10^{24}\ \text{cm}^{-2},\ \text{where } E_{\text{lab}} \text{ is in MeV.}$$

It is important to remark that the uncertainties in the zero-energy parameters are not of appreciable importance in observing shape dependence deviations. When the singlet effective range is found by combining the measurement at 0.4926 MeV with σ_0, a_c, and ϵ_d, the over-all contribution of errors in σ_0, a_c, and ϵ_d to the predicted shape-independent cross section is less than $\pm 0.05\%$ up to 7 MeV as shown in Fig. 2. Thus, the precision of the total cross-section measurements between 0 and 7 MeV is the only limiting factor on the

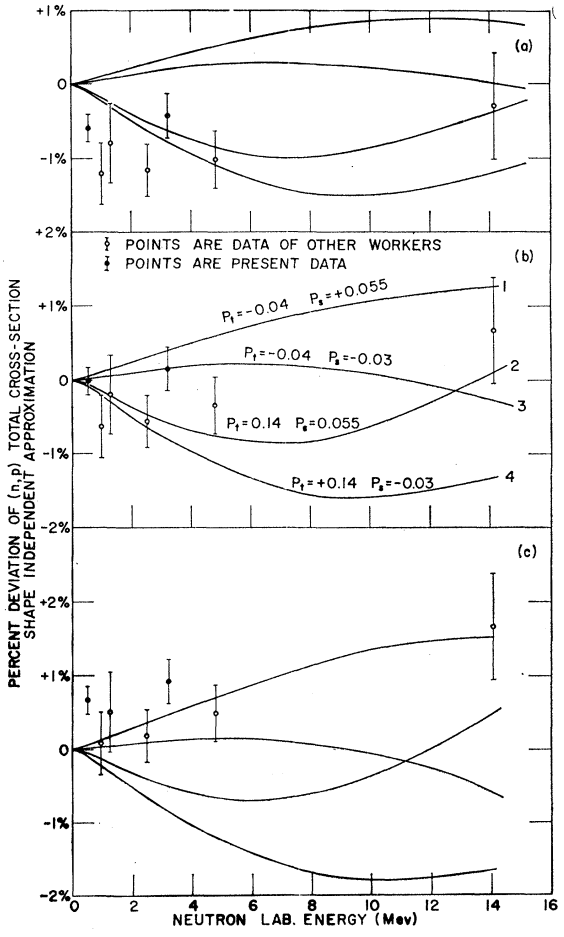

FIG. 15. Comparison of experimental deviations from the shape-independent approximation with those predicted for various values of the shape parameters. (a) Calculated for $r_{0s}=2.80$ F; (b) calculated for $r_{0s}=2.46$ F; (c) calculated for $r_{0s}=2.20$ F.

[21] H. H. Hall, and J. L. Powell, Phys. Rev. **90**, 912 (1953).
[22] Note that these values are based on measurements containing a systematic error. L. Heller, Phys. Rev. **120**, 627 (1960).
[23] R. G. Sachs, *Nuclear Theory* (Addison Wesley Publishing Company, Inc., Reading, Massachusetts, 1953).
[24] L. Heller (private communication).

accuracy with which shape-dependent deviations can be observed up to energies of 7 MeV.

Further measurements in this energy interval are now in progress at Columbia University. However, these measurements will only furnish the sum of the triplet and singlet shape dependent deviations.

To obtain separate values of the singlet and triplet shape parameters P_s and P_t requires both a value of the total cross section near $E_n=17.55\pm0.15$ MeV and a knowledge of the PI and D-wave phase shift. At this energy, the triplet S-wave phase shift passes through 90° so that the contribution of the triplet shape parameter to the expression for the total cross section becomes very small. A precision angular distribution measurement at about the same bombarding energy would, however, be necessary to supply supplementary information about the correction to Eq. (1) required by the no longer inconsequential P- and D-wave contributions. The uncertainties in a_c and σ_0 would also be of importance at 17 MeV.

C. Improvements in experimental technique in both n-p and p-p scattering make it likely that fairly good experimental values of the n-p triplet and singlet shape parameters and the p-p shape parameter will be available within the next two years. A theoretical link has recently been forged from meson theory directly to the shape parameters.[3] The comparison of theoretical values of the n-p singlet shape parameter with presently available experimental data is now under way.[25]

ACKNOWLEDGMENTS

We wish to express our thanks to Professor W. W. Havens, Jr., and Professor L. J. Lidofsky for their advice and encouragement throughout the experiment.

APPENDIX

I. Calculation of Number of Neutrons Detected by a Resonant Detector After a Single Scattering by Hydrogen in the Transmission Sample

Figure 16 shows the path of a neutron produced at an angle θ_1 to the proton beam, at a depth in the lithium target t kV from the point at which forward neutrons have the resonance energy. The neutron's initial energy is a function of t and θ_1, and on scattering through an angle θ it loses a fraction $\sin^2\theta$ of this energy. The element of integration is d^7n, the number of neutrons from a depth between t and $t+dt$ in the neutron producing target, which are scattered at a volume element $d\tau_1$ at r_1, θ_1, ϕ, in the scatterer and are detected in a volume element $d\tau_2$ at r_2, θ_2, ϕ_2, in the resonant detector. The angle of scattering θ and the distance between $d\tau_1$ and $d\tau_2$, r, are convenient auxiliary parameters which in calculation must be expressed by the appropriate functions $r(r_1,r_2,\theta_1,\theta_2,\phi_1,\phi_2)$ and $\theta(r_1,r_2,\theta_1,\theta_2,\phi_1,\phi_2.)$ It can be shown that under the approximations of Sec. IIIB and those listed below:

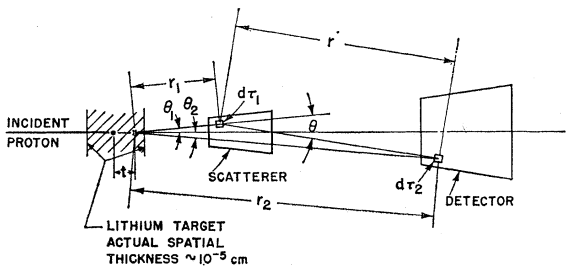

FIG. 16. Coordinates used in the derivation of the number of neutrons detected after a single inscattering.

$$N_{\text{inscattered}} \cong \frac{AT}{\pi} \underbrace{\int\cdots\int}_{\text{sevenfold}} \frac{d\tau_1\, d\tau_2\, dt}{r_1^2 r^2[1+C(t/E_0+\alpha\theta_1^2+\sin^2\theta)^2]}, \quad \text{(I1)}$$

where (1) T is the transmission of the hydrocarbon sample; (2) A is a constant = (number of incident neutrons/steradian, keV of target thickness, sec) × (number of hydrogen atoms per cc in scatterer) × (total cross section of hydrogen at E_0) × (number of detector atoms per cc) × (σ_0 of resonance); (3) $C=(2E_0/\Gamma)^2$; (4) E_0 and Γ are the energy and width of the resonance in the detector cross section; (5) $\alpha\theta_1^2$ gives approximately the fractional decrement in the energy of neutrons produced at θ_1 to the forward direction (for a Li(p,n) target producing 0.5-MeV neutrons $\alpha=0.393$ per rad²); (6) the neutron energy loss on scattering from hydrogen is taken as $E_0\sin^2\theta$; (7) the n-p differential scattering cross section is taken as $(4\cos\theta)\times$(average cross section per steradian); and (8) a minor numerical approximation was made by setting a multiplicative factor of $[\cos^2\theta-(t/E_0)-\alpha\theta_1^2]^{1/2}$ equal to $\cos\theta$ (the maximum error in the integrand due to the approximation is 1%).

II. Correction to Cross Section due to $N_{\text{inscattered}}$

The correction to the measured cross section due to the detection of these inscattered neutrons is

$$\frac{\Delta\sigma_H}{\sigma_H}=\frac{\Delta T_H}{T_H\ln(T_H)}=\frac{(N_{\text{inscattered}}/N_0)}{T_H\ln(T_H)}=\frac{ATI}{N_0\pi T_H\ln(T_H)}, \quad \text{(II1)}$$

where N_0 is the total number of counts/sec detected with the blank in place, I is the sevenfold integral in (1), T is the transmission of the hydrocarbon sample $=T_HT_C$, T_H is the transmission of hydrogen in the

[25] H. P. Noyes (private communication).

sample, T_C is the transmission of carbon in the sample, and T_C is also transmission of carbon blank.

$$N_0=(T_c)\left(\frac{Al_s}{\ln T_H}\right)\int_{\text{fourfold}}\cdots\int\frac{d\tau_2 dt}{r_2^2}\left(\frac{E_0}{E}\right)^{1/2}\times\left(\frac{1}{1+C(t/E_0+\alpha\theta_2^2)^2}\right), \quad \text{(II2)}$$

where l_s is the length of the scatterer. The quantity $(E_0/E)^{1/2}$ varies between 1.005 and 0.995 over the range of integration. The fourfold integral can be performed analytically by setting this factor equal to 1, and setting $\sin\theta_2$ equal to θ_2. A change of variable to $t'=2(t/\Gamma)$ is convenient, and negative values of t are used for energies over E_0. The function obtained is

$$J=2\pi(l_d)\frac{\Gamma}{4\alpha C}\Big[(t'+\theta_m^2\alpha\sqrt{C})\tan^{-1}(t'+\theta_m^2\alpha\sqrt{C})-t'\tan^{-1}t'-\tfrac{1}{2}\ln[1+(t'+\theta_m^2\alpha\sqrt{C})^2]+\tfrac{1}{2}\ln(1+t'^2)\Big]_{t'_{\min}}^{t'_{\max}}, \quad \text{(II3)}$$

where l_d is the length of the detector. This function is also of general interest as it gives the combined effect of target thickness and detector geometry on the shape of resonance curves obtained when the incident particle energy varies with angle.

Substituting the value of N in Eq. (II1) gives

$$d\sigma_H/\sigma_H=I/\pi l_s J. \quad \text{(II4)}$$

PHYSICAL REVIEW VOLUME 129, NUMBER 1 1 JANUARY 1963

Gyromagnetic Ratio of the 2^+ State of Os^{188} *

G. GOLDRING, DRORA KEDEM, AND Z. VAGER
Department of Nuclear Physics, The Weizmann Institute of Science, Rehovoth, Israel

(Received 27 July 1962)

The gyromagnetic ratio of the 2^+ state of Os^{188} of 155 keV excitation was measured by observing the precession in an external magnetic field of the angular distribution of the de-excitation gamma rays following Coulomb excitation with an atomic hydrogen beam. The mean life of the 2^+ state of Os^{188} was also measured by comparing the yield of gamma rays from this level to the yield of gamma rays from the 2^+ state in W^{184}. The mean life of the Os^{188} level was determined to be $\tau=1.05\pm0.10$ nsec, in good agreement with recent direct measurements, and the gyromagnetic ratio was found to be $g=0.20\pm0.02$.

INTRODUCTION

IN a previous communication from this laboratory[1] a measurement of the gyromagnetic ratios of the 2^+ states of the even tungsten isotopes was reported. In that measurement a neutral atomic beam of hydrogen atoms of 1.4 MeV was employed to excite the 2^+ levels, and the angular distribution of the de-excitation gamma rays as well as the angular shift of the distribution pattern in an external magnetic field were observed. A similar measurement was now carried out for the 2^+ state of Os^{188}. Such a measurement, in particular, in conjunction with the tungsten measurements is of interest because Os^{188} is just beyond the region of nuclei of distinctly rotational structure. Another point of a more technical character is that because of the short life-time of the Os^{188} level and the relatively low value of its estimated quadrupole moment, the angular distribution of the gamma rays—at least from a metallic target—may be expected to be very nearly unperturbed.

ANGULAR DISTRIBUTION AND PRECESSION MEASUREMENTS

A metallic target of Os^{188} was prepared in a manner similar to that described in reference 1 for the tungsten targets. The angular distribution and the precession measurements were carried out with protons and hydrogen atoms of 1.45 MeV. The coefficients A_2, A_4 were evaluated for the unperturbed distribution

$$W(\theta)=1+G_2A_2P_2(\cos\theta)+G_4A_4P_4(\cos\theta).$$

The attenuation coefficients are seen to be essentially equal to unity and the distribution can, therefore, be considered unperturbed.

The precession angle in a field of 19.8 ± 0.2 kG was measured in the manner described in reference 1 and was found to be $\omega\tau=0.020\pm0.001$ rad.

As a general check of the method an anisotropic source was simulated by encasing a Co^{57} source in a cylindrical tin absorber, the thickness of which varied with the distance from the source, so as to produce a radiation intensity outside the absorber approximating the angular distribution of the gamma rays from the

* Supported in part by a grant from the Indian Head Mills Inc., New York.

[1] G. Goldring and Z. Vager, Phys. Rev. **127**, 929 (1962).